Available online at www.sciencedirect.com

ScienceDirect

Ceramics International 40 (2014) 8761–8768

CERAMICS INTERNATIONAL

www.elsevier.com/locate/ceramint

Effects of synthesis conditions on the structural, stability and ion conducting properties of $Li_{0.30}(La_{0.50}Ln_{0.50})_{0.567}TiO_3$ (Ln = La, Pr, Nd) solid electrolytes for rechargeable lithium batteries

Karmele Vidal[a,*], Luis Ortega-San-Martín[b], Aitor Larrañaga[a], Rosa Isabel Merino[c], Alodia Orera[c], María Isabel Arriortua[a,*]

[a]Universidad del País Vasco/Euskal Herriko Unibertsitatea, UPV/EHU, Facultad de Ciencia y Tecnología, Apdo. 644, E-48080 Bilbao, Spain
[b]Pontificia Universidad Católica del Perú (PUCP), Departamento de Ciencias, Sección Química, Av. Universitaria 1801, Lima 32, Peru
[c]CSIC-Universidad de Zaragoza, Instituto de Ciencia de Materiales de Aragón, c/Pedro Cerbuna 12, Zaragoza 50009, Spain

Received 22 October 2013; received in revised form 20 January 2014; accepted 20 January 2014
Available online 3 February 2014

Abstract

The structure, thermal stability, morphology and ion conductivity of titanium perovskites with the general formula $Li_{3x}Ln_{2/3-x}TiO_3$ (Ln = rare earth element; $3x = 0.30$) are studied in the context of their possible use as solid electrolyte materials for lithium ion batteries. Materials are prepared by a glycine–nitrate method using different sintering treatments, with a cation-disorder-induced structural transition from tetragonal to cubic symmetry, and are detected as quenching temperature increases. SEM images show that the average grain size increases with increasing sintering temperature and time. Slightly higher bulk conductivity values have been observed for quenched samples sintered at high temperature. Bulk conductivity decreases with the lanthanide ion size. A slight conductivity enhancement, always limited by grain boundaries, is observed for longer sintering times. TDX measurements of the electrolyte/cathode mixtures also show a good stability of the electrolytes in the temperature range of 30–1100 °C.

Keywords: Combustion synthesis; Lithium ion batteries; Lithium-ion conductor; Perovskite structure

1. Introduction

In recent years, solid state lithium ion batteries (LIBs) have attracted considerable attention due to their high power density and safety, as well as their small size and low weight, making these batteries suitable for a broad range of applications, such as cell phones, laptops, cardiac pacemakers and electric vehicles [1]. As an important part of the battery, inorganic solid state electrolytes provide advantages in safety and capacity retention [2]. Several compositions have been studied as possible electrolytes for solid state lithium ion batteries. Thus, lithium tantalate and niobate oxides, lithium based phosphates such as LIPON ($Li_xPO_yN_z$), solid polymer electrolytes (SPE), LISICON type oxides and lithium lanthanum titanates with the general formula $Li_{3x}La_{2/3-x}TiO_3$ (known as LLTO) are among the most promising compounds studied [1,3,4].

Lithium ion-conducting perovskite-type oxides (ABO_3), such as $Li_{3x}La_{2/3-x}TiO_3$, show high ionic conductivities at room temperature (10^{-5}–10^{-3} S cm^{-1}) due to a substantial number of "A" site vacancies in the structure. These vacancies are randomly distributed when Li and La sites are disordered and their presence facilitates the lithium ion transport. Given that a change in the A ions affects conductivity, over the past decade many studies focused on the substitution of ions on either the A site or the B site of the perovskite structure in order to increase the ionic transport, but with little success [5]. The presence of Ti^{4+}, which is "easily" reduced to Ti^{3+} during the charge/discharge process, might result in some

*Corresponding authors. Tel.: +34 946015984; fax: +34 946013500.
E-mail addresses: karmele.vidal@ehu.es (K. Vidal), maribel.arriortua@ehu.es (M.I. Arriortua).

http://dx.doi.org/10.1016/j.ceramint.2014.01.097
0272-8842

electronic conductivity. This effect, that has to be avoided, has reduced the general expectations for this family of compounds as electrolytes [6]. Nevertheless, chemical substitutional studies have been undergoing [7] motivated by the discovery of new applications for LLTO compounds in future LIBs configurations: as cathode coatings [8] or electrolyte separators [9,10]. Regardless the final application of this LLTO family of compounds, it is well known that its microstructure, together with its lithium content, will play a key role in the ionic conductivity of these materials [11,12]. Thus, processing parameters such as sintering temperature, holding time and cooling rate need to be optimized to improve their electrical properties [13]. Until recently, most of the inorganic solid state electrolytes studied (including LLTO family) have been obtained by a solid state reaction. However, this conventional preparation method requires high temperatures and long heating times during the sintering process producing a serious lithium loss and a larger particle size, both negative effects on battery applications. In order to overcome this problem, some alternative synthesis methods, e.g. sol–gel method, microwave sintering and pulsed laser deposition, have been developed to prepare LLTO bulk ceramics or thin films [14,15]. The stability between the perovskite electrolyte and the cathode material during the device fabrication is also an important concern [16], since both LLTO and cathode need to undergo a heat treatment in order to enhance their integration. Therefore, a study of the microstructure stability and the chemical reactions in the interface between the electrolyte and the cathode at high temperature is extremely important.

The present work studies a low temperature synthesis route for some LLTO based perovskites (with the general formula $Li_{0.30}(La_{0.50}Ln_{0.50})_{0.567}TiO_3$, with Ln = La, Pr, Nd), the effects of sintering on their structure and conductivity, as well as their crystal stability and reactivity with a cathode material ($LiMn_2O_4$), in order to develop suitable processing conditions for their eventual use in lithium ion battery systems.

2. Experimental

$Li_{0.30}(La_{0.50}Ln_{0.50})_{0.567}TiO_3$ (Ln = La, Pr, Nd) samples were prepared by the glycine nitrate combustion (GNC) process, a self-combustion technique that uses glycine as fuel and nitrates of the metal components as oxidants. Herein, glycine (Sigma-Aldrich, G7126-500G, > 99%) was added to an aqueous acidified solution containing $LiNO_3$ (Fluka Analytical, 62575-250G-F, ≥ 98%), $La(NO_3)_3 \cdot 6H_2O$ (Fluka Analytical, 61520-100G-F, ≥ 98%), Nd $(NO_3)_3 \cdot 6H_2O$ (Sigma-Aldrich, 289175-25G, ≥ 99.9%), $Pr(NO_3)_3 \cdot 6H_2O$ (Sigma-Aldrich, 205133-50G, 99.9%) and $Ti(C_4H_9O)_4$ (Sigma-Aldrich, 86910-250ML, > 97%) in stoichiometric proportions. The glycine/nitrate molar ratio was adjusted to 1. After drying and self-combustion, the resulting powder was pressed into pellets and annealed in air at 800 °C for 10 h ("raw materials" hereafter). In order to obtain the pure compounds, these raw materials were pressed into pellets and heated at 900 °C for 10 h followed by quenching in air.

For the sintering studies, eight samples of the raw materials with $Li_{0.30}La_{0.567}TiO_3$ composition were fired at 900, 1000, 1100 and 1200 °C for 10 h; four of these new preparations were quenched and the other four were slowly cooled (3 °C/min) at room temperature. Finally, a new series of $Li_{0.30}(La_{0.50}Ln_{0.50})_{0.567}TiO_3$ samples were prepared from the raw materials applying a final sintering temperature of 1200 °C during different times: 30 min, 3 h, 6 h and 10 h, all followed by quenching in air.

Compositional analyses have been carried out on the obtained samples by inductively coupled plasma atomic emission spectroscopy (ICP-AES) on a Horiba Yobin Yvon Activa spectrophotometer (HORIBA, Kyoto, Japan). Prior to measurement, about 50 mg of sample powder was placed in a platinum crucible with 0.6 g of NaOH (Sigma-Aldrich, 55881-500G, ≥ 98%) and fused in a muffle furnace at 500 °C for 15 min. After cooling the crucible, the melted sample was dissolved in Milli-Q Element water acidified with HNO_3.

Room temperature X-ray powder diffraction (XRD) data were collected within the $10° \leq 2\theta \leq 80°$ range with an integration time of 10 s/0.026° step using a Philips X'Pert-PRO X-ray diffractometer (PANalytical, Netherlands) with secondary beam graphite monochromated Cu-Kα radiation. X-ray diffraction data were analysed by the Rietveld method [17] using the GSAS program [18].

Microstructural analysis was carried out on the sintered bars using a JEOL JSM 6400 and a JEOL LSM 7000F (JEOL, Tokyo, Japan) scanning electron microscope at 20 kV and 1.10^{-10} A.

AC electrical measurements were performed from room temperature to 150 °C in air using an impedance analyser (Solartron 1260) in a frequency range 1–10^7 Hz on plane parallel pellets cut from the samples sintered at different temperatures and cooling rates. These pellets were coated with a gold paste (Heraeus, 900.071/145), cured at 550 °C for 0.5 h, and assembled between Pt electrodes. At least two pellets of each composition were measured at room temperature, showing the same conductivity values after being corrected with the corresponding shape factors.

The chemical stability of the LLTO/cathode pairs was studied by mixing the $Li_{0.30}(La_{0.50}Ln_{0.50})_{0.567}TiO_3$ powdered samples with a commercial $LiMn_2O_4$ cathode (Aldrich, particle size < 5 μm) in a 50:50 weight ratio. Thermodiffractometric (TDX) measurements of these mixtures were performed using a Bruker D8 Advance Vantec diffractometer equipped with a platinum sample holder at 30 kV and 20 mA within a range of $10° \leq 2\theta \leq 70°$ (step size = 0.033°). The temperature was increased from room temperature up to 1110 °C (heating rate = 1.8 °C/min), a temperature higher than the conventional co-firing temperatures reported in the literature [19,20].

3. Results and discussion

3.1. Structural study

Fig. 1 shows the Rietveld refinement to the XRD data of the $Li_{0.30}(La_{0.50}Ln_{0.50})_{0.567}TiO_3$ (Ln = La, Pr, Nd) samples obtained from the combustion synthesis after their quenching from 900 °C to room temperature.

All the observed diffraction peaks have been indexed to a perovskite structure with the tetragonal P4/mmm space group.

The tetragonal distortion is attributed to an uneven distribution of vacancies, Li^+ and Ln^{3+} cations over the A1 and A2 crystallographic sites (both 12-fold coordinated with oxygen) in the space group P4/mmm. This unequal distribution, or ordering of these ions, in the A1 and A2 sites leads to the presence of superstructure lines observed on the XRD patterns, which are related to [*hkl*] planes with $l=2n+1$. The presence of these superstructure lines implies the doubling of the perovskite cell parameter in the *c* direction. The quenching of the samples at high temperature increases cation disorder, partially suppressing the A1/A2 alternation along the *c*-axis that is usually observed in slowly cooled compounds [19].

The XRD results also show a decrease in the lattice parameters and unit cell volume, related to the progressive reduction of the averaged ionic radius of the A-site cations (12-fold coordination radii of the lanthanides used are as follows: $r_{(La+3)}=1.36$ Å; $r_{(Pr+3)}=1.30$ Å; $r_{(Nd+3)}=1.27$ Å [21]). This observation is important given that the reduction of the unit cell parameters implies a contraction of the cell and, as a result, the available space for the Li^+ ion hopping may reduce. When this occurs, the result is usually detrimental for the ionic conductivity. Small expansions of the unit cell, as in the case of the La^{3+} and Li^+ substitutions by Sr^{2+} slightly improve conductivity [22,23], but the distortions of the lattice due to substitutions sometimes offset this effect [24].

X-ray diffraction data collected for $Li_{0.30}La_{0.567}TiO_3$ samples after the different sintering treatments (from 900 °C to 1200 °C with and without quenching) are shown in Fig. 2.

As observed, the sintering processes at 900, 1000, 1100 and 1200 °C for the slowly cooled samples produce well-crystallized perovskite-type LLTO phases with the aforementioned superstructure, which can be indexed with the P4/mmm space group. However, the quenched samples show a systematic reduction, to almost disappearance at some temperatures, of the superstructure peaks with increasing quenching temperature. This suggests that as the temperature increases, the cation disorder also increases and the A1/A2 alternation along the *c*-axis is partially suppressed. A fast cooling at 1200 °C produces an XRD pattern without superstructure peaks that can be indexed with a cubic structure (space group, Pm-3m) (Fig. 3), in good agreement with all previous studies [25–29].

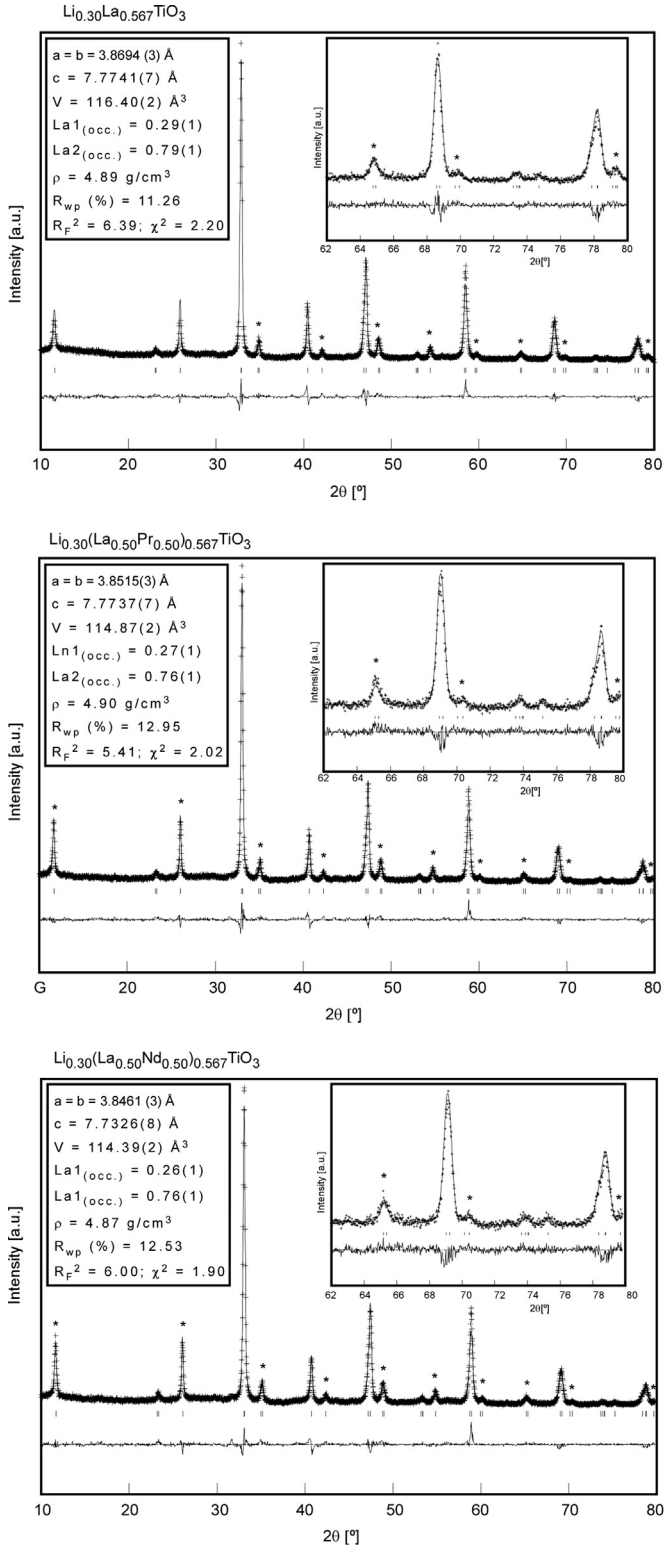

Fig. 1. Rietveld fits of room temperature XRD data for $Li_{0.30}(La_{0.50}Ln_{0.50})_{0.567}TiO_3$ (Ln=La, Pr, Nd) perovskites calcined at 900 °C and quenched to ambient conditions. Superstructure peaks corresponding to the ordering of the Ln ions are indicated by an asterisk (*). Structural parameters obtained by Rietveld refinement are shown in the inset.

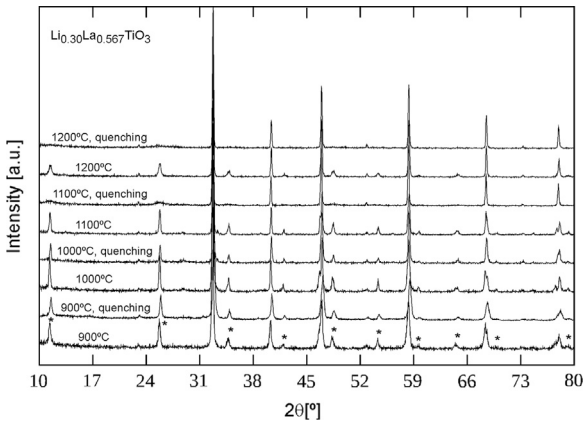

Fig. 2. X-ray diffraction patterns for $Li_{0.30}La_{0.567}TiO_3$ perovskites sintered at different temperatures (900–1200 °C) with and without quenching. Superstructure peaks corresponding to the ordering of the Ln ions are indicated by an asterisk (*).

Final refined values of the structural parameters obtained for the $Li_{0.30}La_{0.567}TiO_3$ samples sintered at different conditions are summarised in Supplementary Tables S1 and S2. The lanthanum occupancies in all cases are summarised in Table 1.

As expected from the preliminary inspection of the XRD data, Table 1 shows important changes in the La^{3+} site occupancies depending on the heat treatments. A drastic change is produced between a sintering temperature of 1100 and 1200 °C for the slowly cooled samples, and a systematic change in the La^{+3} sites population with the temperature is observed for the compounds prepared with quenching. In contrast to the order/disorder effects observed depending on the final treatment, the cell parameters show almost no change.

The ICP-AES elemental composition analysis of the prepared samples (Table 2) indicates that their compositions are very close to the nominal values. Furthermore, the oxides stoichiometry shows no major difference regardless the sintering process or the 1200 °C treatment. It is also important to highlight that the amount of lithium detected stays constant in all cases. This is important because the loss of lithium at high temperatures causes a reduction of the mobile species and thus leads to a deterioration of the grain boundary conductivity [30].

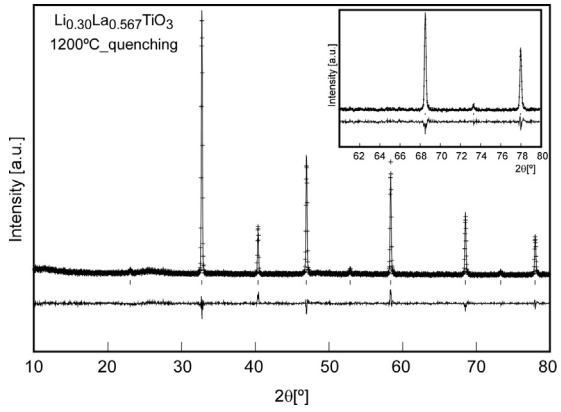

Fig. 3. Rietveld fits of room temperature XRD data for $Li_{0.30}La_{0.567}TiO_3$ perovskites calcined at 1200 °C and quenched to ambient conditions.

Table 1
Occupancies for lanthanum obtained by Rietveld refinement for slowly cooled and quenched $Li_{0.30}La_{0.567}TiO_3$ samples sintered between 900 and 1200 °C.

Parameters	900 °C	1000 °C	1100 °C	1200 °C
$Ln1_{(occ)}$ slowly cooled	0.30(1)	0.28(1)	0.29(1)	0.35(1)
$Ln2_{(occ)}$ slowly cooled	0.83(1)	0.85(1)	0.85(1)	0.78(1)
$Ln1_{(occ)}$ quenched	0.29(1)	0.35(1)	0.49(1)	0.567
$Ln2_{(occ)}$ quenched	0.84(1)	0.78(1)	0.64(1)	

The chemical stability and compatibility of the $Li_{0.30}La_{0.567}TiO_3$ compounds with the commercial $LiMn_2O_4$ electrode were analysed by thermodiffraction and the results are shown in Fig. 4.

Two important processes are noticeable from these data. On one hand, it is clearly observed that superstructure peaks disappear at high temperature. This change takes place at ~930 °C for the $Li_{0.30}La_{0.0567}TiO_3/LiMn_2O_4$ mixture, which is surprising given that when the sample is quenched at 1100 °C the superstructure peaks are clearly present. This result suggests that the traditionally applied quenching process is not fully effective at these temperatures and La^{3+} ions have enough time for reordering.

On the other hand, some new peaks appear above 800 °C. These new peaks, however, do not belong to secondary phases that arise from a chemical reaction between the cathode and the electrolyte; instead these signals come from the $LiMn_2O_4$ spinel reduction reactions that take place around this temperature [31]. In fact, no chemical reaction between both components has been observed up to the maximum temperature. The three $Li_{0.30}(La_{0.50}Ln_{0.50})_{0.567}TiO_3$ compositions display the same structural transformations as the temperature increases (see Supplementary Fig. S1). The main difference between them is the temperature at which the superstructure peaks vanish, slightly smaller (T~900 °C) for Pr^{3+} and Nd^{3+} samples compared with the La^{3+} one.

3.2. Morphological study

The SEM micrographs of the $Li_{0.30}(La_{0.50}Ln_{0.50})_{0.567}TiO_3$ powder samples synthesised by the glycine nitrate combustion method at 900 °C for 10 h and quenched in air are shown in Fig. 5.

On average, these perovskite compositions show a similar microstructure and all grain sizes are below 150 nm. The SEM micrographs taken on the surface of the $Li_{0.30}La_{0.0567}TiO_3$ sintered bars at different temperatures after quenching are shown in Fig. 6.

As expected, SEM micrographs show a noticeable grain size growth (from 150 nm up to ~1 μm) as the sintering temperature rises (from 900 up to 1200 °C). Similar results were observed for the samples prepared without quenching.

Table 2
Summary of the ICP analyses.

Nominal composition	Experimental composition
$Li_{0.30}La_{0.567}TiO_3$	$Li_{0.28(2)}La_{0.55(1)}Ti_{0.99(2)}O_3$
$Li_{0.30}La_{0.283}Nd_{0.283}TiO_3$	$Li_{0.29(2)}La_{0.27(1)}Nd_{0.28(1)}Ti_{1.01(2)}O_3$
$Li_{0.30}La_{0.283}Pr_{0.283}TiO_3$	$Li_{0.29(1)}La_{0.27(1)}Pr_{0.27(1)}Ti_{1.01(2)}O_3$
$Li_{0.30}La_{0.567}TiO_3$ (sintered at 1200 °C with quenching)	$Li_{0.28(1)}La_{0.56(1)}Ti_{1.00(2)}O_3$
$Li_{0.30}La_{0.567}TiO_3$ (sintered at 1200 °C without quenching)	$Li_{0.29(2)}La_{0.57(1)}Ti_{1.02(2)}O_3$

The effect of the sintering time at 1200 °C on the morphology of the samples, measured at the surface of the as-prepared samples, is shown for the $Li_{0.30}La_{0.0567}TiO_3$ composition in Fig. 7.

At 1200 °C, the grain size increases from about 1.2(2) to 2.6(1) μm as the sintering time increases from 30 min to 10 h. Supplementary Fig. S2 shows how the particle growth for samples with Ln=Pr is quite similar. These changes are in good agreement with other published results [32].

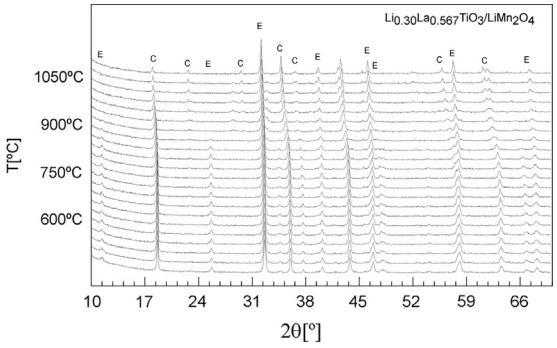

Fig. 4. Thermodiffractometric measurements of the cathode:electrolyte mixture (50% $LiMn_2O_4$:50% $Li_{0.30}La_{0.567}TiO_3$). The diffraction peaks corresponding to the electrolyte and cathode are denoted by E and C, respectively.

3.3. Electrochemical characterisation

All synthesised samples were electrochemically characterised and their total conductivity was evaluated. Such electrochemical properties were studied as a function of the grain size, and as a result by changes on the sintering times and temperatures of the final material.

Pellets of $Li_{0.30}La_{0.567}TiO_3$ prepared at 1000, 1100 and 1200 °C and then quenched resulted in relative densities of 62 (5)%, 96(6)% and 89(5)%, respectively. The reduced density of sample quenched at 900 °C (60%) did not allow a proper conductivity analysis. Fig. 8 shows how the total conductivity of the non-corrected density pellets increases with the sintering temperature. The conductivity of the sample prepared at 1000 °C is two orders of magnitude lower than the others, probably due to the poor densities achieved at that temperature. Given that best

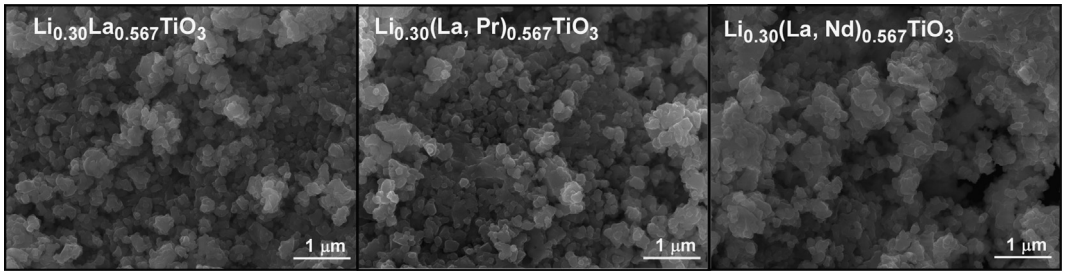

Fig. 5. SEM micrographs taken on the surface of the $Li_{0.30}(La_{0.50}Ln_{0.50})_{0.567}TiO_3$ (Ln=La, Pr, Nd) ceramic pellets obtained at 900 °C with quenching.

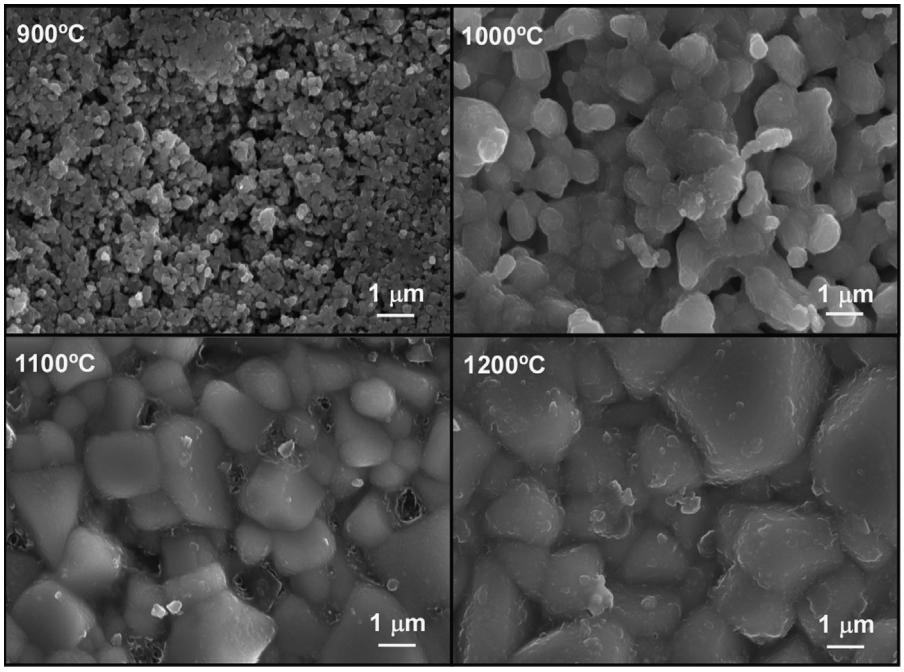

Fig. 6. SEM micrographs taken on the surface of the $Li_{0.30}La_{0.567}TiO_3$ pellets sintered at 900, 1000, 1100 and 1200 °C with quenching.

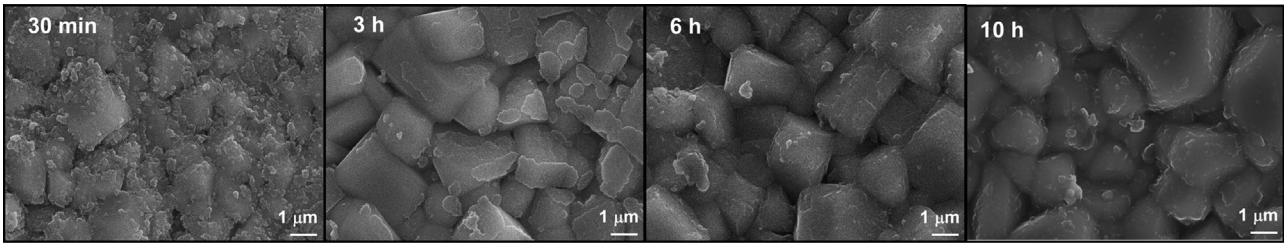

Fig. 7. SEM micrographs taken on the surface of the $Li_{0.30}La_{0.567}TiO_3$ pellets sintered at 1200 °C during 30 min, 3 h, 6 h and 10 h with quenching.

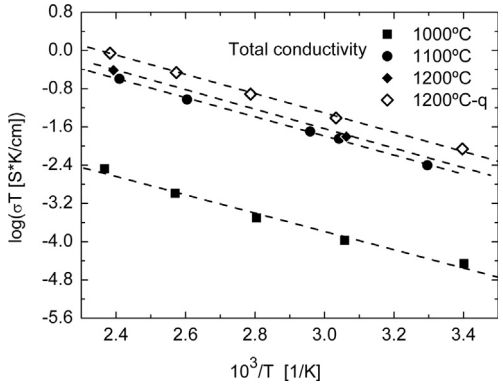

Fig. 8. Arrhenius plots of the total conductivity measured on pellets of $Li_{0.30}La_{0.567}TiO_3$ sintered at 1000, 1100 and 1200 °C, as indicated in the inset. Filled symbols: without quenching and open symbols: sample quenched at 1200 °C.

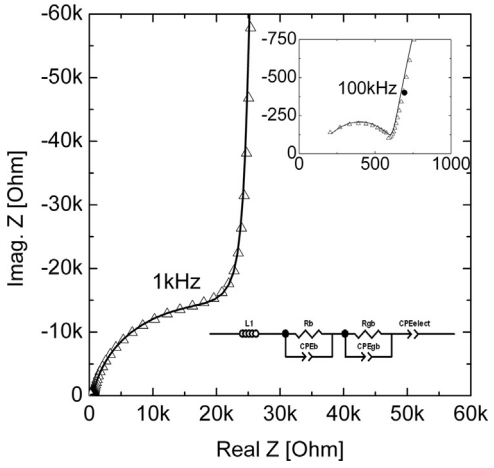

Fig. 9. Impedance plot diagram of $Li_{0.30}La_{0.567}TiO_3$ (sintered at 1200 °C for 6 h and quenched) measured at 22 °C (high frequency range shown in the upper inset). The equivalent circuit used to obtain the conductivity values is depicted at the right hand corner. L1 represents a parasitic inductance due to the experimental setup (~1 μH).

results are observed for those samples sintered at 1200 °C, this sintering temperature was selected for the following tests. Slightly higher conductivity is observed at 22 °C for the sample sintered and quenched at 1200 °C ($\sigma_b = 9 \times 10^{-4}$ S/cm) as compared to the non-quenched sample ($\sigma_b = 6 \times 10^{-4}$ S/cm). However, such differences are not substantial to conclude that quenching is a better option for the synthesis of the sample. These results are in good agreement with the literature [33,34].

Fig. 9 shows a typical impedance diagram at room temperature for $Li_{0.30}La_{0.567}TiO_3$ sintered at 1200 °C for 6 h and quenched in air, where two semicircles are resolved and can be attributed to the bulk (grain interior) contribution (high frequency semicircle with an effective capacitance of ~27 pF/cm) and grain boundary resistance (low frequency semicircle with an effective capacitance of ~5 nF/cm) [35]. The straight line at the low frequency range corresponds to processes of ion-blocking polarisation in the electrodes (Au paste on both sides of the pellets).

Fig. 10 plots the contributions to the total conductivity from both bulk and grain boundary of the three compositions $Li_{0.30}(La_{0.50}Ln_{0.50})_{0.567}TiO_3$ (Ln = La, Pr, Nd) sintered in air at 1200 °C for 6 h, and then quenched. As expected, the bulk (b) and grain boundary (gb) conductivities of all samples increase with temperature, following an Arrhenius behaviour in the whole temperature range measured (25–150 °C) and with higher activation energies for the gb contribution. As the lanthanide size decreases, its conductivity decreases ($\sigma_{La} > \sigma_{Pr} > \sigma_{Nd}$) but its activation energy increases ($E_{a(\sigma b)} = 0.27$, 0.35 and 0.36 eV for La, Pr and Nd, respectively). This trend has also been reported upon complete substitution of La for smaller rare earths [33].

In all cases, the conduction across the grain boundaries limits the total conductivity of the sample, so a more careful study was performed in order to minimize this contribution. In this sense, different sintering times (30 min, 3 h, 6 h and 10 h) were tested and the influence on the electrical grain boundary conductivities was studied (the total contribution of the boundaries to the conductivity and the specific conductivity).

The specific grain boundary conductivity is obtained by multiplying the total contribution of the grain boundaries by a factor d/D, where d is the size of the grain boundary and D is the grain size [36]. Assuming that the dielectric constant of the boundaries equals that of the bulk, d/D is estimated from the equivalent capacitances of the high frequency (HF) and low frequency (LF) impedance arcs as $d/D = C_b/C_{gb} = C_{HF}/C_{LF}$. In all cases, the bulk conductivity remains unchanged with the sintering time, and so does the specific grain boundary conductivity. This fact implies that the nature of these grain boundaries does not change and segregation or degradation processes are unlikely. However, there is a slight enhancement of the total contribution of the grain boundary conductivity for longer sintering times, as shown in Fig. 11, due to an increase of the grain size (see Fig. 7) and consequent decrease of the number of grain boundaries.

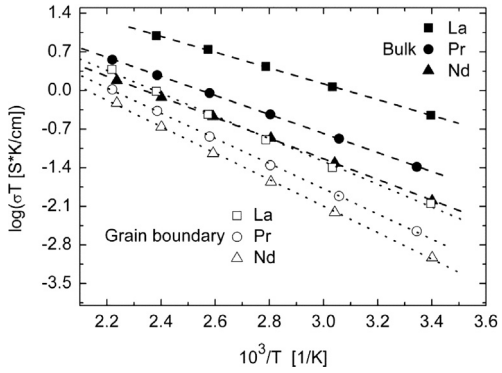

Fig. 10. Arrhenius plots of the bulk and grain boundary contributions to the conductivity of $Li_{0.30}(La_{0.50}Ln_{0.50})_{0.567}TiO_3$ (Ln=La, Pr, Nd), sintered at 1200 °C for 6 h and quenched. Both conductivities have been calculated using the sample's geometrical factor length/surface.

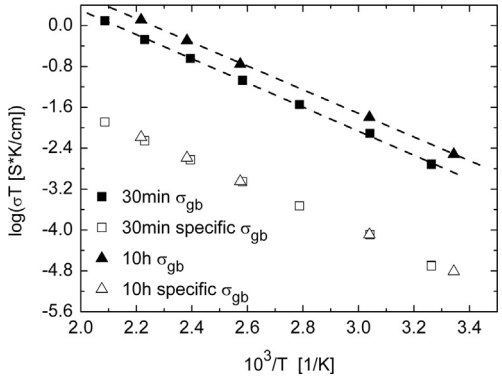

Fig. 11. Arrhenius plots of the grain boundary contribution to the conductivity of $Li_{0.30}(La_{0.50}Pr_{0.50})_{0.567}TiO_3$ sintered at 1200 °C for 30 min and 10 h and quenched in air. The grain boundary contribution ($\sigma_{gb}=(1/R_{gb})\cdot(l/S)$) and the specific grain boundary conductivity ($\sigma_{gb}=d/D$) are represented.

4. Conclusions

The structure and thermal stability of a series of titanium perovskites with the general formula $Li_{0.30}(La_{0.50}Ln_{0.50})_{0.567}TiO_3$ (Ln=La, Pr, Nd) prepared by the glycine–nitrate method have been studied as a material that can be used in lithium ion batteries. Calcination of the powders at 900 °C followed by quenching produces well-crystallized perovskite-type LLTO phases with a partially ordered structure (P4/mmm space group). The chemical reactivity between these compounds and commercial cathode material ($LiMn_2O_4$) has been analysed by TDX measurements within a 30–1100 °C temperature range. No secondary phases were detected even at the highest temperature used, showing that all phases were stable and chemically compatible. The conductivity values decrease as the lanthanide size decreases. This is probably a result of two simultaneous effects: the contraction of the unit cell volume (and thus the reduction of the available space for the Li^+ ion transport) and the increase in the A-site disorder (a well studied parameter in other perovskite-type compounds). $Li_{3x}Ln_{2/3-x}TiO_3$ pellets were prepared at different sintering conditions and cooling rates in order to study how the preparation conditions affect their structural, morphological and electrochemical properties. It was observed that the tetragonal superlattice lines gradually disappear when the quenching temperature is raised (900–1200 °C). Some of the superlattice peaks disappeared at lower temperature than quenched experiments reported in the published literature. This result indicates that the usual quenching techniques are not that effective in keeping the exact high temperature structure. SEM images show how the average grain size increases in direct proportion to the sintering temperature and time, as expected. Slightly higher values of conductivity have been obtained for quenched samples, but not significant enough to favour the quenching process over slow cooling synthesis. A slight enhancement of the total contribution of the grain boundary conductivity has been obtained for longer sintering times.

Acknowledgements

This research has been funded by the Consejería de Industria, Innovación, Comercio y Turismo (SAIOTEK 2012 programmes), by Dpto. Educación, Política Lingüística y Cultura of the Basque Goverment (Grupos de Investigación del Sistema Universitario Vasco 2013–2018; IT-630-13), by Ministerio de Ciencia e Innovación (MAT2010-15375 and MAT2012-30763) and by Ministerio de Economía y Fondos Feder (MAT2010-19837-C06-06). The authors thank SGIker technical support (UPV/EHU, MEC, GV/EJ and European Social Fund). L.O.S.M. acknowledges the Departamento Ciencias, PUCP, for the allocation of research time.

Appendix A. Supporting information

Supplementary data associated with this article can be found in the online version at http://dx.doi.org/10.1016/j.ceramint.2014.01.097.

References

[1] J.F.M. Oudenhoven, L. Baggetto, P.H.L. Notten, Adv. Energy Mater. 1 (2011) 10–33.
[2] J. Wang, Y. Li, X. Sun, Nano Energy 2 (2013) 443–467.
[3] A. Patil, V. Patil, D.W. Shin, J.W. Choi, D.S. Paik, S.J. Yoon, Mater. Res. Bull. 43 (2008) 1913–1942.
[4] B. Scrosati, J. Garche, J. Power Sources 195 (2010) 2419–2430.
[5] S. Stramare, W. Wepper, Mater. Sci. Eng. B 113 (2004) 85–90.
[6] O. Bohnke, Solid State Ion. 179 (2008) 9–15.
[7] K.P. Abhilash, P.C. Selvin, B. Nalini, P. Nithyadharseni, B.C. Pillari, Ceram. Int. 39 (2013) 947–952.
[8] D. Qian, B. Xu, H.M. Cho, T. Hatsukade, K.J. Carroll, Y.S. Meng, Chem. Mater. 24 (2012) 2744–2751.
[9] Y. Inaguma, M. Nakashima, J. Power Sources 228 (2013) 250–255.
[10] Y. Liang, L. Ji, B. Guo, Z. Lin, Y. Yao, Y. Li, M. Alcoutlabi, Y. Qiu, X. Zhang, J. Power Sources 196 (2011) 436–441.
[11] H. Geng, J. Lan, A. Mei, Y. Lin, C.W. Nan, Electrochim. Acta 56 (2011) 3406–3414.
[12] A. Mei, Q.M. Jiang, Y.H. Lin, C.W. Nan, J. Alloys Compd. 486 (2009) 871–875.
[13] H.X. Geng, A. Mei, C. Dong, Y.H. Lin, C.W. Nan, J. Alloys Compd. 481 (2009) 555–558.
[14] C.R. Milian, T. Mariño, E. Pérez, O.L. Alves, P. Aranda, M. Aguilar, Y. Mosqueda, Ceram. Int. 40 (2013) 249–256.
[15] J.M. Li, T. Qiu, Int. J. Miner. Metall. Mater. 19 (2012) 245–251.

[16] C.L. Liao, C.H. Wen, K.Z. Fung, J. Alloys Compd. 432 (2007) L22–L25.
[17] H.M. Rietveld, J. Appl. Crystallogr. 2 (1969) 65–71.
[18] A.C. Larson, R.B. Von Dreele, , 1994 (Los Alamos National Laboratory report LAUR 86-748).
[19] Z. Quan, S. Ohguchi, M. Kawase, H. Tanimura, N. Sonoyama, J. Power Sources 244 (2013) 375–381.
[20] D. Guo, Z. Chang, B. Li, H. Tang, X.Z. Yuan, H. Wang, Solid State Ion. 237 (2013) 34–39.
[21] R.D. Shannon, Acta Crystallogr. A32 (1976) 751–767.
[22] J.-S. Lee, K.S. Yoo, T.S. Kim, H.J. Jung, Solid State Ion. 98 (1997) 15–26.
[23] Y. Kawakami, H. Ikuta, M. Wakihara, J. Solid State Electrochem. 2 (1998) 206–210.
[24] S. Stramare, V. Thangadurai, W. Weppner, Chem. Mater. 15 (2003) 3974–3990.
[25] O. Bohnke, H. Duroy, J.L. Fourquet, S. Ronchetti, D. Mazza, Solid State Ion. 149 (2002) 217–226.
[26] N.N. Dinh, P.D. Long, L.D. Trong, Commun. Phys. 14 (2004) 90–94.
[27] A.C. Sutorik, M. Green, C. Cooper, J. Wolfenstine, G. Gilde, J. Mater. Sci. 47 (2012) 6992–7002.
[28] M. Catti, M. Sommariva, R.M. Ibberson, J. Mater. Chem. 17 (2007) 1300–1307.
[29] A. Várez, J. Ibarra, A. Rivera, C. León, J. Santamaría, M.A. Laguna, M.L. Sanjuán, Chem. Mater. 15 (2003) 225–232.
[30] H. Geng, A. Mei, T. Lin, C. Nan, Mater. Sci. Eng. B 164 (2009) 91–95.
[31] S. Komaba, S.N. Yabuuchi, S. Ikemoto, J. Solid State Chem. 183 (2012) 234–241.
[32] H.X. Geng, A. Mei, C. Dong, Y.H. Lin, C.W. Nan, J. Alloys Compd. 481 (2009) 555–558.
[33] S. Stramare, V. Thangadurai, W. Weppner, Chem. Mater. 15 (2003) 3974–3990.
[34] K.Y. Yang, J.W. Wang, K.Z. Fung, J. Alloys Compd. 458 (2008) 415–424.
[35] J.T.S. Irvine, D.C. Sinclair, A.R. West, Adv. Mater. 2 (1990) 132–138.
[36] X. Guo, R. Waser, Mater. Sci. 51 (2006) 151–210.